

# Two-Dimensional Multifunctional Materials from Endohedral Fullerenes

Jie Li and Ruqian Wu\*

*Department of Physics and Astronomy, University of California, Irvine, California 92697-4575, USA.*

**ABSTRACT:** A new multifunctional 2D material is theoretically predicted based on systematic ab-initio calculations and model simulations for the honeycomb lattice of endohedral fullerene  $W@C_{28}$  molecules. It has structural bistability, ferroelectricity, multiple magnetic phases, and excellent valley characters and can be easily functionalized by the proximity effect with magnetic isolators such as  $MnTiO_3$ . Furthermore, we may also manipulate the valley Hall and spin transport properties by selectively switch a few  $W@C_{28}$  molecules to the metastable phase. These findings pave a new way in integrate different functions in a single 2D material for technological innovations.

**KEYWORDS:** multifunctional 2D materials, vertical ferroelectricity, valley Hall effect, endohedral fullerenes.

\* E-mail: [wur@uci.edu](mailto:wur@uci.edu).

With diverse new physical properties, two-dimensional (2D) materials have attracted extensive research interest ever since the successful exfoliation and synthesis of graphene.<sup>1</sup> A large variety of 2D materials have been predicted, fabricated and characterized, from insulators (e.g, hexagonal boron nitride<sup>2</sup>), semiconductors (e.g., and silicene,<sup>3</sup> germanene,<sup>4</sup> phosphorene,<sup>5</sup> transition metal dichalcogenides,<sup>6</sup> Cr<sub>2</sub>Ge<sub>2</sub>Te<sub>6</sub>,<sup>7</sup> CrI<sub>3</sub>,<sup>8</sup> and stanene<sup>9</sup>), to semimetals (e.g. TiS<sub>2</sub>,<sup>10</sup> 1T-MoTe<sub>2</sub>,<sup>11</sup> and Ta<sub>2</sub>Se<sub>3</sub><sup>12</sup>). These materials manifest many emergent quantum properties such as high carrier mobility, quantum spin Hall effect (QSHE), quantum anomalous Hall effect (QAHE), valley-polarized anomalous Hall effect (VAHE), and low-dimensional ferromagnetic ordering. However, multifunctional 2D materials with two or more exotic features in a single system have rarely been reported.

Fullerenes, such as C<sub>60</sub>, C<sub>72</sub>, and C<sub>80</sub>, have been extensively studied in the last two decades.<sup>13-15</sup> Research interest in these systems resurges as endohedral fullerenes with additional metal atoms, ions, or clusters embedded in the closed mesh (denoted as M@C<sub>n</sub>) offer new possibility of producing diverse exotic properties by adjusting the metal cores.<sup>16-19</sup> Small endohedral fullerenes are particularly interesting as they may easily provide environments with low symmetry for metal atoms and hence may develop ferroelectricity, a desired feature for the electric control. Both pristine and endohedral C<sub>28</sub> molecules have been recently synthesized in experiments,<sup>20</sup> they can be hence used as building blocks for the construction of innovative 2D materials.<sup>21,22</sup>

In this paper, we propose a new series of 2D ferroelectric and valleytronic materials: a simple honeycomb lattice of endohedral W@C<sub>28</sub> molecules. Through systematic ab-initio calculations and model simulations, we found that 2D W@C<sub>28</sub> honeycomb lattice is an excellent multifunctional 2D material that combines structural bistability, ferroelectricity, multiple magnetic

phases, and large valley splitting. Even the ground state of the free-standing  $W@C_{28}$  lattice is nonmagnetic, a large valley spin splitting of  $\sim 55$  meV for VAHE and a robust QAHE can be induced when it is functionalized by a magnetic  $MnTiO_3$  substrate. On the other hand, the metastable magnetic phase has sizeable magnetic moment ( $1 \mu_B$ /molecule) and magnetic anisotropy energy (MAE, 1.09 meV/molecule). As the W atom is ionized in the  $C_{28}$  cage, we may switch  $W@C_{28}$  molecules between the two phases and manipulate the magnetic state and valley Hall current with a local electric field, which is ideal for high speed and energy efficient control. These findings pave a way for developing novel multifunctional 2D vdW materials that are essential for technological innovations.

Many endohedral  $C_{28}$  ( $M@C_{28}$ ) molecules have been synthesized in carbon vapor,<sup>20</sup> which enriched the fullerene chemistry<sup>18,19</sup> and justifies the material choice in the present work. W is selected as it has large spin orbit coupling (SOC) and possesses magnetic moment in environment with weak interactions. Interestingly, our DFT calculations show that the  $W@C_{28}$  molecule has two stable structures (denoted as phase I and II in following discussions). As shown in Figure 1a, the W atom displaces by 0.85 Å between these two phases, and the phase I has an energy advantage of 0.131 eV. From the climbing image nudged elastic band (CINEB) calculations, the forward (phase I  $\rightarrow$  II) and backward (phase II  $\rightarrow$  I) transitions have energy barriers of 0.198 eV and 0.067 eV, respectively. DFT calculations further show that the  $W@C_{28}$  molecule has a magnetic moment of  $2.0 \mu_B$  in both phases. To determine their magnetic anisotropy energies, we determine the torque  $T(\theta)$  as a function of the polar angle  $\theta$  between the magnetization and the z axis as shown in Figure 1b.<sup>23,24</sup> By integrating  $T(\theta)$ , we obtain the angular dependence of energy,  $E(\theta)$ . One may see that the highest and lowest energies occur at  $\theta=0^\circ$  and  $\theta=90^\circ$ , indicating that

both phases have an in-plane easy axis with the energy differences ( $MAE = E(\theta = 90^\circ) - E(\theta = 0^\circ)$ ) of -0.56 meV and -0.95 meV, respectively. Curves of the projected density of states (PDOS) shown in Figure 1c reveal that the in-plane MAEs mostly stem from the cross-spin SOC interaction between  $d_{xy\uparrow}$  and  $d_{(x^2-y^2)\downarrow}$  orbitals of tungsten. In addition, it appears that all W d-orbitals hybridize with carbon atoms and the highest occupied molecular orbital (HOMO) of  $W@C_{28}$  switches from a basically pure C state in phase I to a W-C intermixed state in phase II. As  $W@C_{28}$  molecules are transferable, we expect that they can be used as magnetic superatoms to functionalize other materials such as graphene and topological materials.

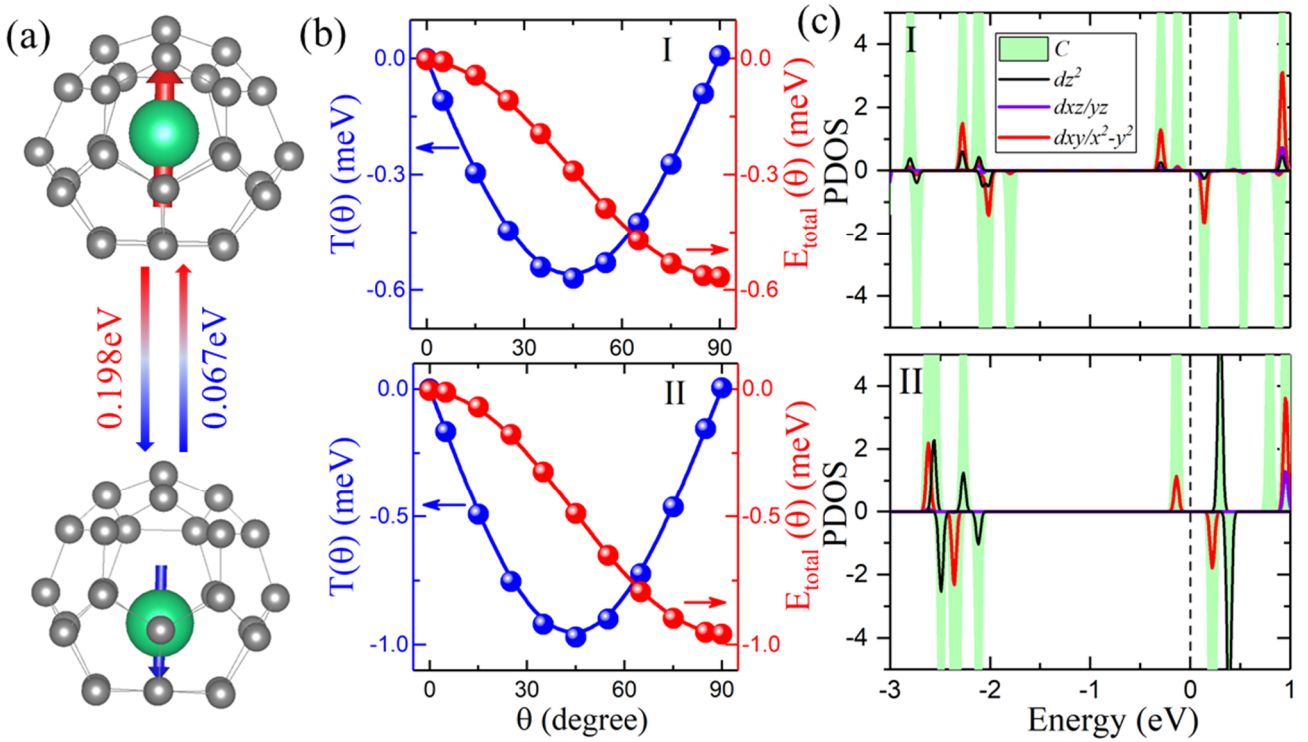


Figure 1. (a) Schematic structure of  $W@C_{28}$  in phases I and II. Two colored arrows represent the direction of the dipoles. (b) Calculated torque vs the angle  $\theta$  for  $W@C_{28}$ . (c) The corresponding PDOS of  $W@C_{28}$ .

In this work, we focus on properties of a  $W@C_{28}$  honeycomb lattice as a new functional 2D

material. W@C<sub>28</sub> molecules have the C<sub>3v</sub> symmetry and it is nature to perceive that they may form either hexagonal or honeycomb structure on appropriate substrates. From our calculations, the honeycomb structure shown in Figure 2a is more stable than the hexagonal structure for a free-standing W@C<sub>28</sub> monolayer, with a gain of 0.314 eV in binding energy, which is defined as

$$E_b = E_{mol} - E_{2D}/n \quad (1)$$

Here,  $E_{mol}$  and  $E_{2D}$  are the total energies of the isolated W@C<sub>28</sub> and the 2D crystal; and  $n$  is the number of W@C<sub>28</sub> molecules per unit cell. Note that the 2D W@C<sub>28</sub> lattice (2D-W@C<sub>28</sub>) has a binding energy as large as 4.61 eV per molecule, indicating strong interactions among W@C<sub>28</sub> molecules and decent possibility of synthesizing the 2D-W@C<sub>28</sub> honeycomb lattice in experiments.

The high thermal and dynamic stability of the 2D-W@C<sub>28</sub> honeycomb lattice is examined by phonon calculations and ab initio molecular dynamics (AIMD) simulations. The corresponding phonon bands in Figure S2a show the absence of imaginary frequency branch, indicating that the system is dynamically stable. Furthermore, we keep the 2D-W@C<sub>28</sub> molecules in a 4×4 supercell (928 atoms/supercell) for 10ps (5000 steps) at 300K through AIMD simulations and results show no sign of structure destruction. The total energy fluctuates in a small range without noticeable jump (see Figure S2b in the Supporting Information). Therefore, we believe that 2D-W@C<sub>28</sub> honeycomb lattice is thermally stable at least up to room temperature. After structural relaxation, the lattice constant in the lateral plane is 10.67Å (a=b). DFT calculations show that 2D-W@C<sub>28</sub> also has two stable structures as shown in Figure 2c, and the atomic displacement and energy barriers are somewhat enhanced from those for the free molecule, to 0.99 Å and 0.56 eV (0.12 eV for backward switch), respectively (see more details in Figure S3 in the Supporting Information).

As W donates electrons to the  $C_{28}$  cage, there are net electric polarizations in the  $2D-W@C_{28}$  lattice. The calculated electric dipoles for  $2D-W@C_{28}$  are around  $-0.706 \text{ e}\text{\AA}$  and  $0.683 \text{ e}\text{\AA}$  per unit cell in phases I and II, respectively. The opposite electric dipole moments indicate that  $2D-W@C_{28}$  is a new ferroelectric material as well. It is striking that the polarization can be switched by a reasonably small external electric field. As shown in Figure 3d, a structural phase transition (from I to II) occurs when an external electric field of  $0.3 \text{ V/\AA}$  is applied.

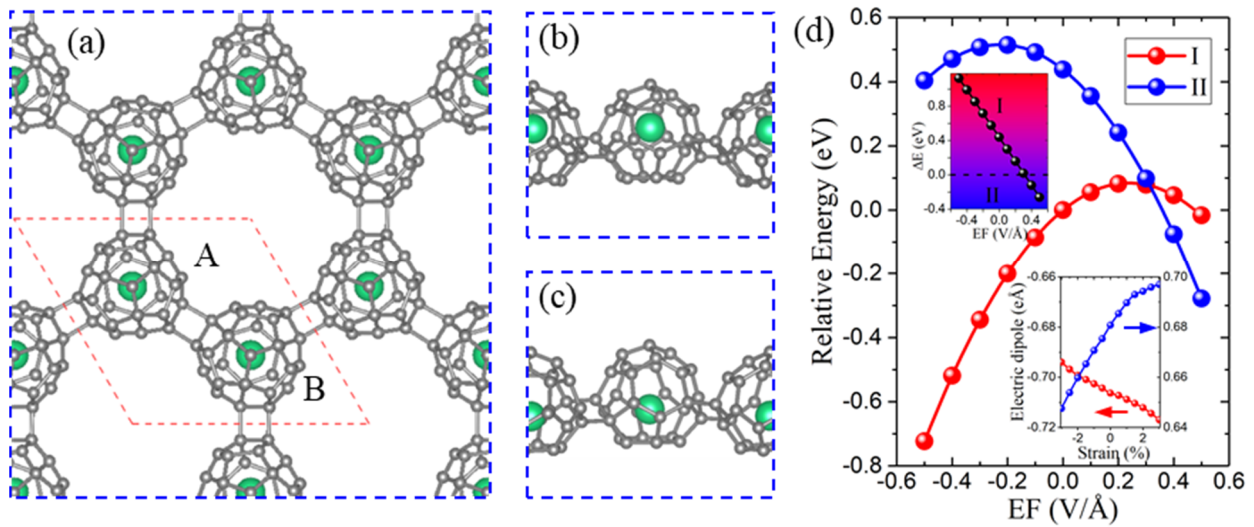


Figure 2. (a) Top views of  $2D-W@C_{28}$  (the red dashed quadrangle shows the supercell for calculations). (b) (c) Side views of  $2D-W@C_{28}$  in phases I and II, respectively. (d) The relative energy of  $2D-W@C_{28}$  in phases I and II as functions of the external electric field (negative external electric field is along  $z$  axis), the inset are the energy differences as functions of the external electric field and the electric dipoles as functions of strain.

It is known that all ferroelectric materials have piezoelectric properties as well. Here, we further investigate the piezoelectric property of  $2D-W@C_{28}$  by calculating its electric dipole as a function of an in-plane stain. In the inset of Figure 2d, one may see that the electric dipoles indeed depend on the strain, particularly for the phase II. Thus,  $2D-W@C_{28}$  as a new ferroelectric

material may have a wide range of technological applications, such as non-volatile memories, field effect transistors and sensors.

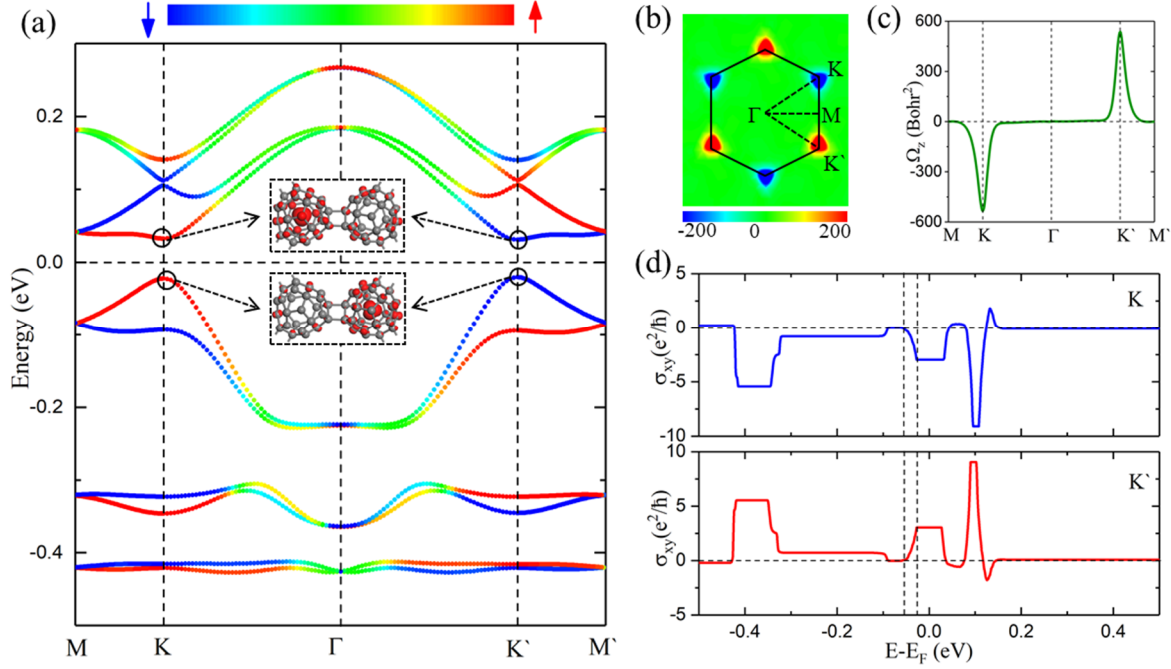


Figure 3. (a) The band structure of 2D-W@C<sub>28</sub> with SOC. (Inset are the band decomposed charge density of VBM and CBM at K and K' point, with an isosurface value of 0.001 e/Å<sup>3</sup>). (b) (c) Calculated Berry curvature of 2D-W@C<sub>28</sub> over 2D Brillouin zone and along high symmetry lines, respectively. (d) The anomalous Hall conductivity  $\sigma_{xy}$  as a function of Fermi level.

In the phase I, the W atom of 2D-W@C<sub>28</sub> obviously shifts toward the dome and the symmetry is reduced. DFT calculations show that 2D-W@C<sub>28</sub> is a nonmagnetic semiconductor in phase I, due to the strong intermolecular interactions. Considering the strong SOC of tungsten, we first examine if 2D-W@C<sub>28</sub> is topologically nontrivial. As shown in Figure S5, the calculated  $Z_2$  is zero so 2D-W@C<sub>28</sub> is not a topological material by itself. Nonetheless, 2D-W@C<sub>28</sub> can be an excellent valleytronic material or can become a topological material after being functionalized by others. To examine this possibility, we may analyze its band structure in Figure 3 and PDOS in

Figure S4. There is a large band gap of  $\sim 55$  meV at both K and K' points with opposite spins because of strong SOC of W. The band decomposed charge densities show that holes and electrons residing at K and K' valleys are from the A and B sublattices, respectively. The PDOS curves show that electronic states near to Fermi level contain the  $d_{xz/yz}$  orbitals of W and  $p_{x/y}$  orbitals of carbon. The map of Berry curvature,  $\Omega(\mathbf{k})$ , of 2D-W@C<sub>28</sub> in the 2D Brillouin zone (BZ) and along the high symmetric lines are shown in Figure 3b,c. Obviously,  $\Omega(\mathbf{k})$  has the same magnitude but opposite signs around the K and K' points, similar to the feature of pristine TMD monolayers and graphene. Quantitatively, we give the Hall conductivity as a function of the position of the Fermi level by integrating  $\Omega(\mathbf{k})$  over vicinities around the K and K' valleys and summing over states below  $E_F$ , i.e.,  $\sigma_{xy} = \sum_{n \in occ} \frac{e^2}{h} \int_{K \text{ or } K'} \Omega_n(\mathbf{k}) \frac{dk}{(2\pi)^2} = C_{K \text{ or } K'} \frac{e^2}{h}$ . Due to the valley degeneracy,  $C_K$  and  $C_{K'}$  exactly cancel each other in the entire energy range as seen in Figure 3d, but each of them is nonetheless remarkably close  $\pm 3$ . Obviously, 2D-W@C<sub>28</sub> has many important features of topological or valleytronic materials and we may attain net valley Hall currents or even QAHE with some modifications.

Among numerous ways of engineering the valley and topological properties, the proximity effect is probably the most intuitive one and has been extensively used in previous studies.<sup>25-27</sup> Here, we use MnTiO<sub>3</sub>, a potential linear magnetoelectric material, as the substrate to magnetize 2D-W@C<sub>28</sub>. Our DFT calculations show that the bulk MnTiO<sub>3</sub> is an antiferromagnetic insulator with a band gap of  $\sim 1$  eV. A MnTiO<sub>3</sub> (001) slab with 12 layers of atoms is used to mimic the substrate, and the surface is terminated by Mn atoms as shown in Figure 4a. We use a  $2 \times 2$  supercell in the lateral plane and fix the in-plane lattice constant to MnTiO<sub>3</sub>, which leads to a lattice mismatch of 3.8% with 2D-W@C<sub>28</sub>. All atoms except the bottom six MnTiO<sub>3</sub> layers are

relaxed through DFT calculations. DFT calculations indicate that each Mn atom in the surface layer has a large spin magnetic moment of  $\sim 4.5 \mu_B$ . This produces a noticeable spin polarization in 2D-W@C<sub>28</sub>, even though the net magnetic moment of each C atom still appear to be small ( $\sim 0.01 \mu_B$ ).

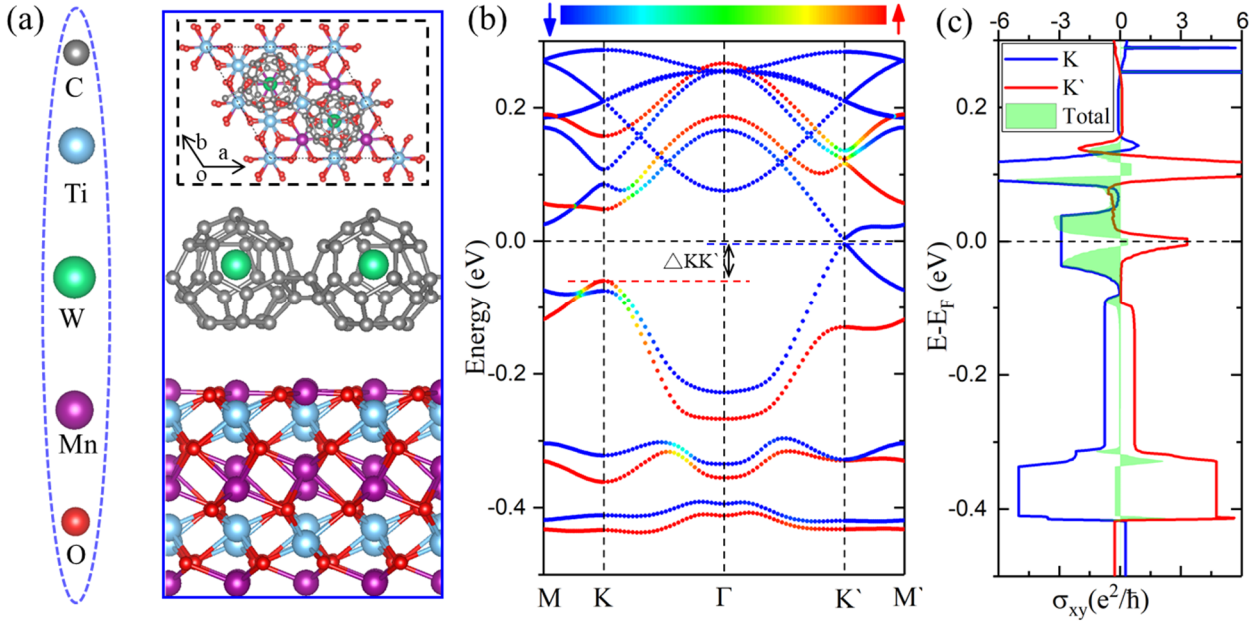


Figure 4. (a) The side view of structure of 2D-W@C<sub>28</sub> on MnTiO<sub>3</sub> (001) surface. (Inset is the top view). (b) The calculated band structure of 2D-W@C<sub>28</sub> on MnTiO<sub>3</sub> (001) surface. (The valley splitting  $\Delta_{KK'} = E_K - E_{K'}$ , where  $E_K$  ( $E_{K'}$ ) represents VBM at K ( $K'$ ) point). (c) The corresponding anomalous Hall conductivity  $\sigma_{xy}$  as a function of Fermi level.

Let us first focus on the valley splitting. As the valley and spin degrees of freedom are interlocked, the proximity effect of the magnetic MnTiO<sub>3</sub> substrate on the two valleys is nonequivalent, as seen in the band structure of 2D-W@C<sub>28</sub>/MnTiO<sub>3</sub> in Figure 4b. A large valley splitting ( $\Delta_{KK'}$ ) of  $\sim 55$  meV and a reasonable band gap ( $\sim 8.8$  meV) at the  $K'$  valley can be found. To shed some light on the large valley splitting due to the interplay of the proximity effect,

broken symmetry and strong SOC, we construct a  $k \cdot p$  model for 2D-W@C<sub>28</sub> (see more details in the Supporting Information). By fitting the DFT results, the corresponding parameters are extracted as shown in Table S1 in Supplemental Information. The strong SOC parameters ( $\lambda_V$ ,  $\lambda_C$ ) in both valence band and conduction band are mainly from contributions of W atoms. Negative  $\lambda_C$  changes the spin orders between the valence band and conduction band.<sup>28</sup> The large effective exchange fields for valence bands show the robust proximity effect from the substrate, which induces a sizable valley splitting.

Because the degeneracy between two valleys is broken, we may selectively use carriers from different valleys, e.g., by shifting the Fermi level to below the valence band maximum (VBM) at the K or K' points with a bias. A net orbital magnetic moment ( $m_v$ ) associated with the valley index<sup>31</sup> is plotted as a function of the position of the Fermi level in Figure S6. Obviously, the valley-polarized anomalous Hall effect is analogous to the QAHE, and falls into the same category as the Berry-phase related topological transport phenomena. The anomalous Hall conductivity as a function of the position of the Fermi level is shown in Figure 4c. Note that the net Chern number takes a value of -3 as we sweep the Fermi level up and down by merely 0.02 eV so the QAHE can be easily realized in this system.

DFT calculations show that 2D-W@C<sub>28</sub> in phase II is metallic and has a magnetic moment of  $\sim 2 \mu_B$  per unit cell (see in the band structure of 2D-W@C<sub>28</sub> in phase II in Figure S7) and a large MAE of  $\sim 2.18$  meV per unit cell as shown in Figure S8a. By using the renormalized spin-wave theory (RSWT),<sup>29,30</sup> we calculate its Curie temperature (the renormalized magnetization  $M(T)/M(0)$  as a function of  $T$  is shown in Figure S8b, and  $T_c$  is determined by the location where the renormalized magnetization drops zero). One may see that 2D-W@C<sub>28</sub> in phase II has

exceedingly high Curie temperatures of  $\sim 167\text{K}$ , a new van der Waals type metallic 2D magnetic material. Furthermore, we may use  $\text{W}@C_{28}$  molecules in phase II as magnetic dopants for the control of transport properties of the phase-I  $\text{W}@C_{28}$  lattice. To this end, we propose a conceptual device shown in Figure S9 to produce the VAHE. Using silicon as the substrate as well as the channel for applying the bias, a few  $\text{W}@C_{28}$  molecules in the Hall bar can be selectively switched to the phase II. When the distance between adjacent magnetic molecules is shorter than the spin mean free path, they are expected to produce valley anomalous Hall effect with the same mechanism as discussed above for  $2\text{D-}\text{W}@C_{28}/\text{MnTiO}_3$ . This idea can be proven to some extent by the band structure of  $2\text{D-}\text{W}@C_{28}$  in Figure S10 with 25% molecules in the phase II, in which the degeneracy between the two valleys is clearly lifted. The advantage of this device is obvious as there is no need to change chemical ingredients and the distribution of “dopants” can be easily reprogrammed.

In summary, we proposed a new 2D ferroelectric and valleytronic material based on endohedral fullerenes  $C_{28}$  and further explored its structural and electronic properties through systematic ab-initio calculations and model simulations. The results show that  $2\text{D-}\text{W}@C_{28}$  has structural bistability, ferroelectricity, multiple magnetic phases, and excellent valley characters. In the ground state nonmagnetic phase, a large valley spin splitting of  $\sim 55\text{ meV}$  can be induced by the proximity effect from the  $\text{MnTiO}_3$  substrate, which offers the possibility for developing a new series of valleytronic materials. Furthermore, we proposed a new strategy to use local electric field for the manipulation of valley Hall current, based on the exotic ferroelectric property and multiple magnetic phases of  $\text{W}@C_{28}$ . These studies suggest a way for producing novel 2D multifunctional materials for diverse applications.

**Methods.** All the density functional theory (DFT) calculations in this work were carried out with the Vienna ab-initio simulation package (VASP) at the level of the spin-polarized generalized-gradient approximation (GGA).<sup>32</sup> The interaction between valence electrons and ionic cores was considered within the framework of the projector augmented wave (PAW) method.<sup>33,34</sup> The energy cutoff for the plane wave basis expansion was set to 500 eV. A Hubbard  $U = 2.0$  eV was added to the 5b orbitals of tungsten (W) for the correlation effect. The vdW correction (DFT-D3) was included in all calculations.<sup>35</sup> All atoms were fully relaxed using the conjugated gradient method for the energy minimization until the force on each atom became smaller than  $0.01$  eV/Å, and the criterion for total energy convergence was set at  $10^{-5}$  eV.

## ACKNOWLEDGMENTS

Work was supported by US DOE, Basic Energy Science (Grant No. DE-FG02-05ER46237).

Calculations were performed on parallel computers at NERSC.

## REFERENCES

- (1) Novoselov, K. S.; Geim, A. K.; Morozov, S. V.; Jiang, D.; Zhang, Y.; Dubonos, S. V.; Grigorieva, I. V.; Firsov, A. A. Electric field effect in atomically thin carbon films. *Science* **2004**, *306* (5696), 666.
- (2) Dean, C. R.; Young, A. F.; Meric, I.; Lee, C.; Wang, L.; Sorgenfrei, S.; Watanabe, K.; Taniguchi, T.; Kim, P.; Shepard, K. L.; Hone, J. Boron nitride substrates for high-quality graphene electronics. *Nature Nanotech* **2010**, *5* (10), 722.
- (3) Cahangirov, S.; Topsakal, M.; Aktürk, E.; Şahin, H.; Ciraci, S. Two- and one-dimensional honeycomb structures of silicon and germanium. *Phys. Rev. Lett.* **2009**, *102* (23), 236804.
- (4) Li, L.; Lu, S. Z.; Pan, J.; Qin, Z.; Wang, Y. Q.; Wang, Y.; Cao, G. Y.; Du, S.; Gao, H. J. Buckled germanene formation on Pt(111). *Adv. Mater.* **2014**, *26*, 4820.
- (5) Liu, H.; Neal, A. T.; Zhu, Z.; Luo, Z.; Xu, X.; Tománek, D.; Ye, P. D. Phosphorene: an unexplored 2D semiconductor with a high hole mobility. *ACS Nano* **2014**, *8* (4), 4033.
- (6) Wang, Q. H.; Kalantar-Zadeh, K.; Kis, A.; Coleman, J. N.; Strano, M. S. Electronics and optoelectronics of two-dimensional transition metal dichalcogenides. *Nature Nanotech* **2012**, *7*, 699.
- (7) Gong, C.; Li, L.; Li, Z.; Ji, H.; Stern, A.; Xia, Y.; Cao, T.; Bao, W.; Wang, C.; Wang, Y.; Qiu, Z. Q.; Cava, R. J.; Louie, S. G.; Xia, J.; Zhang, X. Discovery of intrinsic ferromagnetism in two-dimensional van der Waals crystals. *Nature* **2017**, *546*, 265.
- (8) Huang, B.; Clark, G.; Navarro-Moratalla, E.; Klein, D. R.; Cheng, R.; Seyler, K. L.; Zhong, D.; Schmidgall, E.; McGuire, M. A.; Cobden, D. H.; Yao, W.; Xiao, D.; Jarillo-Herrero, P.; Xu, X. Layer-dependent ferromagnetism in a van der Waals crystal down to the monolayer limit. *Nature* **2017**, *546*, 270.
- (9) Zhu, F.; Chen, W.; Xu, Y.; Gao, C.; Guan, D.; Liu, C.; Qian, D.; Zhang, S.; Jia, J. F. Epitaxial growth of two-dimensional stanene. *Nature Mater* **2015**, *14*, 1020.
- (10) Zhu, Z.; Zou, Y.; Hu, W.; Li, Y.; Gu, Y.; Cao, B.; Guo, N.; Wang, L.; Song, J.; Zhang, S.; Gu, H.; Zeng, H. Near-infrared plasmonic 2D semimetals for applications in communication and biology. *Adv. Funct. Mater.* **2016**, *26*, 1793.
- (11) Qi, Y.; Naumov, P. G.; Ali, M. N.; Rajamathi, C. R.; Schnelle, W.; Barkalov, O.; Hanfland,

- M.; Wu, S. C.; Shekhar, C.; Sun, Y.; Suss, V.; Schmidt, M.; Schwarz, U.; Pippel, E.; Werner, P.; Hillebrand, R.; Forster, T.; Kampert, E.; Parkin, S.; Cava, R. J.; Felser, C.; Yan, B.; Medvedev, S. A. Superconductivity in Weyl semimetal candidate MoTe<sub>2</sub>. *Nat. Commun.* **2016**, *7*, 11038.
- (12) Ma, Y.; Jing, Y.; Heine, T. Double Dirac point semimetal in 2D material: Ta<sub>2</sub>Se<sub>3</sub>. *2D Mater.* **2017**, *4*, 025111.
- (13) *The fullerenes*; Kroto, H. W., Fischer, J. E., Cox, D. E., Eds.; Pergamon Press Ltd: Oxford, 1993.
- (14) *Fullerenes: from synthesis to optoelectronic properties*; Guldi, D. M.; Martin, N., Eds.; Kluwer Academic Publishers: Dodrecht, The Netherlands, 2002.
- (15) Kroto, H. W. The stability of the fullerenes C<sub>n</sub>, with n = 24, 28, 32, 36, 50, 60 and 70. *Nature*, **1987**, *329*, 529
- (16) Popov, A. A.; Yang, S. F.; Dunsch, L. Endohedral fullerenes. *Chem. Rev.* **2013**, *113* (8), 5989.
- (17) Bethune, D. S.; Johnson, R. D.; Salem, J. R.; de Vries, M. S.; Yannoni, C. S. Atoms in carbon cages: the structure and properties of endohedral fullerenes. *Nature* **1993**, *366*, 123.
- (18) Romero, N. A.; Kim, J.; Martin, R. M. Electronic structures and superconductivity of endohedrally doped C<sub>28</sub> solids from first principles. *Phys. Rev. B* **2007**, *76*, 205405.
- (19) Dognon, J.; Clavaguéra, C.; Pyykkö, P. A Predicted organometallic series following a 32-electron principle: An@C<sub>28</sub> (An = Th, Pa<sup>+</sup>, U<sup>2+</sup>, Pu<sup>4+</sup>). *J. Am. Chem. Soc.* **2009**, *131*, 238.
- (20) Dunk, P. W.; Kaiser, N. K.; Mulet-Gas, M.; Rodríguez-Forteza, A.; Poblet, J. M.; Shinohara, H.; Hendrickson, C. L.; Marshall, A. G.; Kroto, H. W. The Smallest Stable Fullerene, M@C<sub>28</sub> (M = Ti, Zr, U): Stabilization and Growth from Carbon Vapor. *J. Am. Chem. Soc.* **2012**, *134*, 9380.
- (21) Enyashin, A.; Gemming, S.; Heine, T.; Seifert, G.; Zhechkov, L. C<sub>28</sub> fullerites-structure, electronic properties and intercalates. *Phys. Chem. Chem. Phys.* **2006**, *8*, 3320.
- (22) Zeng, J.; Zhang, Y.; Qin, W.; Cui, P.; Yan, Q.; Zhang, Z. Varying topological properties of two-dimensional honeycomb lattices composed of endohedral fullerenes. *Phys. Rev. B* **2019**, *100*, 045143.
- (23) Wang, X. D.; Wu, R. Q.; Wang, D. S.; Freeman, A. J. Torque method for the theoretical determination of magnetocrystalline anisotropy. *Phys. Rev. B* **1996**, *54*, 61.
- (24) Hu, J.; Wu, R. Q. Control of the magnetism and magnetic anisotropy of a single-molecule

magnet with an electric field. *Phys. Rev. Lett.* **2013**, *110*, 097202.

(25) Qi, J.; Li, X.; Niu, Q.; Feng, J. Giant and tunable valley degeneracy splitting in MoTe<sub>2</sub>. *Phys. Rev. B* **2015**, *92*, 121403(R).

(26) Zhang, Q.; Yang, S. A.; Mi, W.; Cheng, Y.; Schwingenschlögl, U. Large spin-valley polarization in monolayer MoTe<sub>2</sub> on top of EuO(111). *Adv. Mater.* **2016**, *28*, 959.

(27) Zhao, C.; Norden, T.; Zhang, P.; Zhao, P.; Cheng, Y.; Sun, F.; Parry, J. P.; Taheri, P.; Wang, J.; Yang, Y.; Scrace, T.; Kang, K.; Yang, S.; Miao, G.; Sabirianov, R.; Kioseoglou, G.; Huang, W.; Petrou, A.; Zeng, H. Enhanced valley splitting in monolayer WSe<sub>2</sub> due to magnetic exchange field. *Nature Nanotech* **2017**, *12*, 757.

(28) Liu, G. B.; Shan, W.Y.; Yao, Y.G.; Yao, W.; Xiao, D. Three-band tight-binding model for monolayers of group-VIB transition metal dichalcogenides. *Phys. Rev. B* **2013**, *88*, 085433.

(29) Bloch, M. Magnon renormalization in ferromagnets near the Curie point. *Phys. Rev. Lett.* **1962**, *9* (7), 286-287.

(30) Li, Z.; Cao, T.; Louie, S. G. Two-dimensional ferromagnetism in few-layer van der Waals crystals: renormalized spin-wave theory and calculations. *J. Magn. Magn. Mater.* **2018**, *463*, 28-35.

(31) Xiao, D.; Yao, W.; Niu, Q. Valley-contrasting physics in graphene: magnetic moment and topological transport. *Phys. Rev. Lett.* **2007**, *99*, 236809.

(32) Perdew, J. P.; Burke, K.; Ernzerhof, M. Generalized gradient approximation made simple. *Phys. Rev. Lett.* **1996**, *77*, 3865.

(33) Blochl, P. E. Projector augmented-wave method. *Phys. Rev. B* **1994**, *50*, 17953.

(34) Kresse, G.; Joubert, D. From ultrasoft pseudopotentials to the projector augmented-wave method. *Phys. Rev. B* **1999**, *59*, 1758.

(35) Grimme, S.; Antony, J.; Ehrlich, S.; Krieg, S. A consistent and accurate ab initio parametrization of density functional dispersion correction (DFT-D) for the 94 elements H-Pu. *J. Chem. Phys.* **2010**, *132*, 154104.